Journal of Materials Chemistry C

ROYAL SOCIETY OF CHEMISTRY

COMMUNICATION

View Article Online
View Journal | View Issue

Cite this: J. Mater. Chem. C, 2023, 11, 2469

Received 21st November 2022,
Accepted 26th January 2023

DOI: 10.1039/d2tc04952j

rsc.li/materials-c

Indole-fused BN-heteroarenes as narrowband blue emitters for organic light-emitting diodes†

Cheng-Zhuo Du,‡[a] Yang Lv,‡[a] Hengyi Dai,[b] Xiangchen Hong,[b] Jianping Zhou,[b] Ji-Kun Li,[a] Rong-Rong Gao,[a] Dongdong Zhang,*[b] Lian Duan[bc] and Xiao-Ye Wang*[ad]

A new family of indole-fused multi-resonance thermally activated delayed fluorescence materials have been developed, which exhibit narrowband blue emission with a small full width at half maximum of 22–23 nm. High maximum external quantum efficiencies of up to 16.8% have been achieved in organic light-emitting diodes. Furthermore, it is unveiled that peripheral substitutions can not only promote device efficiency but also help to maintain narrowband emission under high dopant concentrations.

In order to realize wide color gamut displays to meet the BT.2020 standard in organic light-emitting diodes (OLEDs), it is of great significance to develop organic luminescent materials with high efficiency and narrowband emission.[1] A remarkable milestone in the field of OLEDs is the development of thermally activated delayed fluorescence (TADF) materials based on donor–acceptor type molecules, which can achieve 100% internal quantum efficiency by rapid reverse intersystem crossing (RISC) induced by a small singlet–triplet energy gap (ΔE_{ST}).[2] However, the severe vibrational coupling between the ground state and the excited state, as well as the structural relaxation of the excited state, inevitably leads to spectral broadening,[3,4] resulting in poor color purity of TADF materials. To achieve narrowband emission, in 2016, Hatakeyama *et al.* developed multi-resonance TADF (MR-TADF) materials to facilitate significant separation of frontier molecular orbitals (FMOs) through the opposite resonance effects of boron and nitrogen atoms.[5] Small ΔE_{ST} and suppressed vibrational coupling were achieved, ensuring the realization of high efficiency and narrowband emission simultaneously.

Owing to the distinctive advantages of MR-TADF materials, a number of MR emitters have been developed prosperously in recent years.[6–14] Notably, carbazole-fused MR backbone CzBN, as a representative MR core, has been widely used due to its merits of easy functionalization, narrowband emission and high photoluminescence quantum yields (Φ_{PL}) (Fig. 1).[15–19] Thus, a wide variety of high-performance narrowband OLEDs have been reported based on CzBN derivatives, realizing multi-color emission from sky-blue to yellow regions.[19–33] Despite these significant advancements, it is still challenging to achieve blue emission *via* simple structural modification of CzBN due to the large π-conjugated plane of the carbazole segment.[5,34–37] Considering the limited variety of blue MR-TADF emitters, it is of great significance to develop novel MR backbones to enrich the molecular library of blue-emitting MR materials with high color purity.

Herein, we synthesize a novel indole-fused MR-TADF skeleton (InBN) *via* π-truncation of CzBN to achieve narrowband blue emission (Fig. 1). Compared with CzBN, the new framework based on indole not only maintains the MR effect, but also achieves narrowband blue-shifted emission with smaller full width at half maximum (FWHM). The peripheral substituents on the bottom benzene ring at the *para* position to boron are introduced to further modulate the photophysical properties

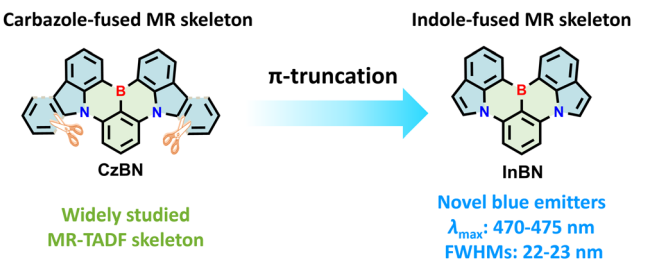

Fig. 1 Molecular design strategy of indole-fused MR-TADF emitters.

[a] State Key Laboratory of Elemento-Organic Chemistry, Frontiers Science Center for New Organic Matter, College of Chemistry, Nankai University, Tianjin 300071, China. E-mail: xiaoye.wang@nankai.edu.cn; Web: http://wang.nankai.edu.cn
[b] Key Lab of Organic Optoelectronics and Molecular Engineering of Ministry of Education, Department of Chemistry, Tsinghua University, Beijing 100084, China. E-mail: ddzhang@mail.tsinghua.edu.cn
[c] Center for Flexible Electronics Technology, Tsinghua University, Beijing 100084, China
[d] State Key Laboratory of Luminescent Materials and Devices, South China University of Technology, 510640 Guangzhou, China

† Electronic supplementary information (ESI) available: Experimental details, synthetic procedures, characterization data, NMR spectra, theoretical calculations and electroluminescence data. See DOI: https://doi.org/10.1039/d2tc04952j

‡ These authors contributed equally.

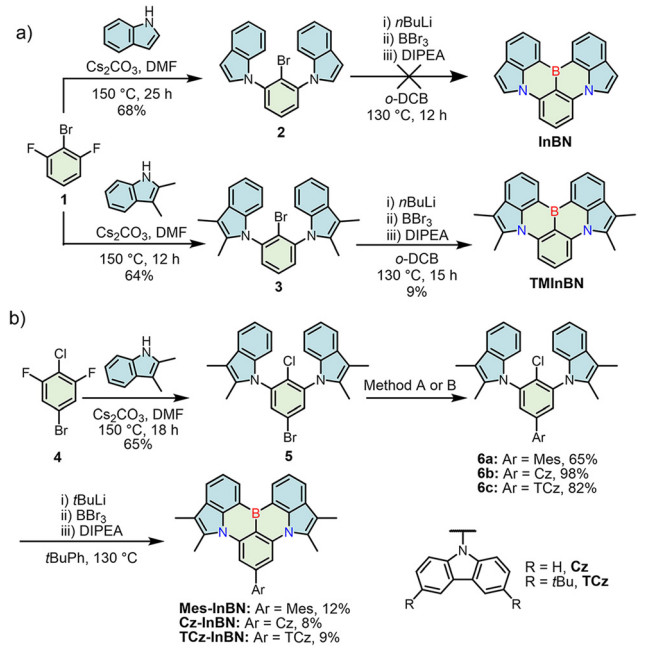

Scheme 1 Synthetic routes to indole-fused MR emitters. Method A: mesitylboronic acid, $Pd(PPh_3)_4$, K_2CO_3, THF/H_2O, 75 °C, 20 h; method B: carbazole or 3,6-di-*tert*-butylcarbazole, $Pd(OAc)_2$, $P(tBu)_3{\cdot}HBF_4$, *t*BuONa, *o*-xylene, 130 °C.

without compromising the narrowband emission feature. These indole-fused emitters exhibit sharp blue emission with the maxima at 470–475 nm and small FWHMs of 22–23 nm along with high Φ_{PL} of 66–70%. The TADF-sensitized OLED devices based on these new emitters exhibit the highest maximum external quantum efficiency (EQE_{max}) of up to 16.8% with a small FWHM of 29 nm. It is also observed that peripheral substitutions on the InBN core can suppress spectral broadening in the doped films with high dopant concentrations. This work expands the diversity of blue MR-TADF materials and provides new concepts for designing novel BN-heteroarenes with tunable light-emitting properties.

The synthetic routes to indole-fused MR emitters are shown in Scheme 1. Initially, we directly employed indole for the synthesis of the InBN skeleton. A nucleophilic aromatic substitution between 2-bromo-1,3-difluorobenzene (**1**) and indole gave precursor **2**, but the following borylation failed to produce the target compound, probably owing to the reactive β-position of indole during the electrophilic borylation step (Scheme 1a).[38] Thus, we introduced additional methyl groups on the reactive sites of indole, and successfully obtained the target compound TMInBN through the same synthetic route. To finely modulate the photophysical properties, a widely adopted strategy is to introduce substituents, which can additionally suppress the solid-state aggregation.[24,27–29,31,32] Therefore, Mes-InBN, Cz-InBN and TCz-InBN were synthesized from the key precursors **6a**, **6b**, and **6c**, which were obtained from 5-bromo-2-chloro-1,3-difluorobenzene (**4**) in high yields by aromatic nucleophilic substitution and the subsequent Pd-catalyzed Suzuki or Buchwald–Hartwig coupling reactions (Scheme 1b).

Thermal gravimetric analysis (TGA) reveals that these indole-based emitters possess excellent thermal stability with decomposition temperatures (T_d) ranging from 365 to 446 °C (Fig. S1, ESI†), which lays the ground for vacuum thermal deposition during OLED fabrication. According to the measurement results of differential pulse voltammograms (DPV) (Fig. S9, ESI†), the highest occupied molecular orbital (HOMO) and the lowest unoccupied molecular orbital (LUMO) energy levels are calculated to be −5.35 eV and −2.54 eV for TMInBN, −5.38 eV and −2.52 eV for Mes-InBN, −5.51 eV and −2.58 eV for Cz-InBN, and −5.52 eV and −2.56 eV for TCz-InBN, respectively. The corresponding electrochemical energy gaps were deduced as 2.81 eV, 2.86 eV, 2.93 eV, and 2.96 eV, respectively. The electronic properties of Mes-InBN and TMInBN are similar, while the introduction of the electron-donating carbazole moiety can further enlarge the electrochemical energy gap.

Time-dependent density functional theory (TD-DFT) calculations were performed at the B3LYP/6-311G(d,p) level to further shed light on the electronic properties. The HOMO and LUMO distributions, energy gaps, and oscillator strengths are shown in Fig. 2. The HOMOs are mainly located on the nitrogen and carbon atoms at the *meta* position relative to the boron atom, while the LUMOs are principally distributed on the boron atom as well as at its *ortho* and *para* positions in the InBN core. All these emitters share identical HOMO/LUMO distribution, which is similar to that of CzBN,[24] indicating that the MR effect can be well maintained after π-truncation. It is also observed that the mesityl (Mes) substituent in Mes-InBN does not participate in the FMO distribution owing to the large dihedral angle between the Mes group and the InBN core. In terms of Cz-InBN and TCz-InBN, only LUMO distributions slightly extend to the nitrogen atoms of carbazole. It is therefore

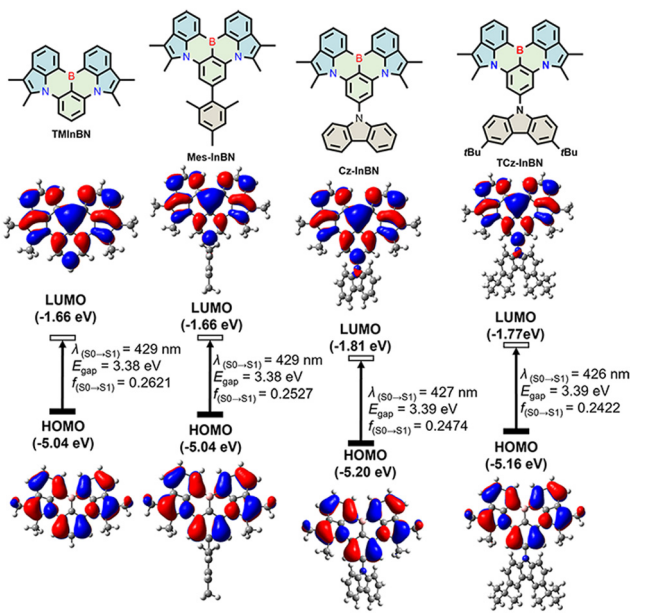

Fig. 2 Calculated HOMO and LUMO distributions, energy levels, HOMO–LUMO gaps, and oscillator strengths of TMInBN, Mes-InBN, Cz-InBN, and TCz-InBN.

anticipated that the peripheral steric groups only have little influence on the electronic properties, which, on the other hand, may act as inert bulk substituents to suppress intermolecular interactions in the solid state. The calculated energy levels of these emitters show a similar trend to the electrochemical results (Fig. S9, ESI†). According to the optimized geometries, the root-mean-square deviation (RMSD) values between S_0 and S_1 states are calculated as 0.57 Å, 0.67 Å, 0.67 Å, and 0.65 Å for TMInBN, Mes-InBN, Cz-InBN, and TCz-InBN, respectively (Fig. S10, ESI†). These results demonstrate that there is weak vibrational coupling between the ground state and the excited state, which facilitates narrowband emission and small Stokes shifts.

The photophysical properties of these compounds were studied in dilute toluene solutions (1×10^{-5} M, Fig. 3), and the detailed data are summarized in Table 1. TMInBN, Mes-InBN, Cz-InBN, and TCz-InBN show similar absorption bands peaking at 462, 461, 457, and 456 nm, respectively. They all exhibit intense blue fluorescence with sharp emission peaks at 475, 475, 470 and 470 nm, and small FWHMs of 23, 23, 22, and 22 nm, respectively, implying that the peripheral steric substituents barely compromise the color purity. These four emitters exhibit almost identical absorption spectra in different solvents, but their emission spectra show obvious red-shifted maxima upon increasing the solvent polarities gradually from cyclohexane to dichloromethane, confirming the short-range charge transfer characteristics (Fig. S2, S3 and Table S1, ESI†).[27] Compared with the other two emitters, Cz-InBN and TCz-InBN show slightly blue-shifted emission maxima. The reason can be attributed to the reduction of the electron-withdrawing ability of boron atoms due to the *para*-positioned carbazole units.[22] Moreover, small Stokes shifts are obtained as 13, 14, 13 and 14 nm for TMInBN, Mes-InBN, Cz-InBN, and TCz-InBN, respectively, suggesting that there are negligible structural changes between the ground state and the excited state. Moreover, only small differences in Φ_{PL} of the four MR emitters are observed, proving that the peripheral substituents barely affect the luminescence performance. The photophysical properties of TMInBN, Mes-InBN, Cz-InBN, and TCz-InBN in 9-3-(9*H*-carbazol-9-yl)phenyl)-9*H*-3,9′-bicarbazole (mCPBC) were further examined (Fig. S5–S7, ESI†). As the dopant concentration increases, the emission maxima of TMInBN are slightly red-shifted and the spectra are broadened, accompanied by significantly decreased Φ_{PL}. The concentration-caused emission quenching and spectral broadening are suppressed in Mes-InBN, Cz-InBN, and TCz-InBN doped films, indicating that the steric substituents can suppress intermolecular interactions to prevent aggregation-caused emission quenching and spectral broadening. In addition, the transient PL spectra of the doped films at different temperatures were recorded (Fig. S8, ESI†). The lifetimes of the delayed fluorescence gradually decrease with increasing temperature from 100 to 300 K, demonstrating a typical TADF characteristic.

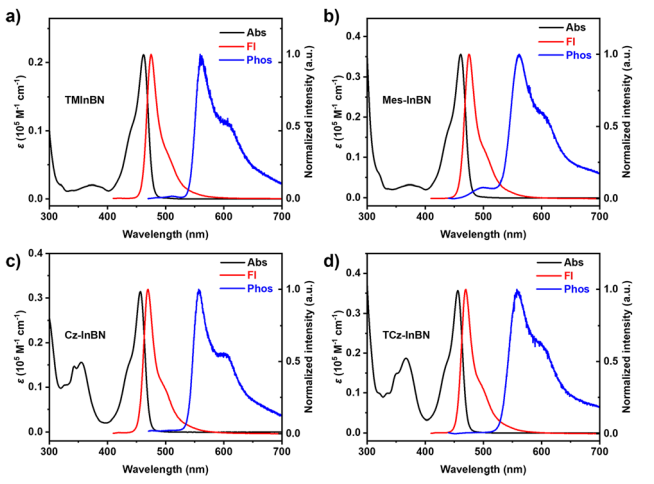

Fig. 3 UV-vis absorption (black line), normalized fluorescence (red line, λ_{ex}: 400 nm), and phosphorescence (blue line, λ_{ex}: 420 nm, delay: 25 ms) spectra of (a) TMInBN, (b) Mes-InBN, (c) Cz-InBN, and (d) TCz-InBN in toluene solution (1×10^{-5} M).

To gain deeper insight into the TADF characteristic, the phosphorescence spectra and transient photoluminescence decay curves of these emitters were also measured. The singlet and triplet energies are calculated from the emission peaks of the fluorescence and phosphorescence spectra, respectively. The ΔE_{ST} values are obtained as 0.39, 0.40, 0.41, and 0.42 eV for TMInBN, Mes-InBN, Cz-InBN, and TCz-InBN, respectively, which are larger than those of most reported MR compounds.[6,7] The highly correlated Spin-Component Scaling second-order approximate Coupled-Cluster (SCS-CC2) calculation was performed to theoretically estimate ΔE_{ST},[39] which are obtained as 0.30, 0.29, 0.30 and 0.29 eV for TMInBN, Mes-InBN, Cz-InBN, and TCz-InBN, respectively (Table S4, ESI†). Therefore, the spin–orbit coupling (SOC) matrix elements between the triplet (T_n) and singlet states (S_1) were calculated to evaluate the RISC process from T_n to S_1 (Fig. S11, ESI†). Obviously, for all four compounds, the SOC constants between T_1 and S_1 are relatively very small (0.014, 0.014, 0.042, and 0.028 cm^{-1} for TMInBN, Mes-InBN, Cz-InBN, and TCz-InBN, respectively), while the upper-lying triplet states may play an important role in the whole RISC process.[37,40–44] According to the quantum yields and lifetimes of prompt and delayed components (Fig. S4, ESI†), the radiative decay rate (k_r), intersystem crossing (k_{ISC}) and reverse intersystem crossing (k_{RISC}) constants of these MR emitters are calculated and summarized in Table 1. Benefiting from the rigid structure, these indole-fused emitters possess high k_r values of up to 8.9×10^7 s^{-1}, while the relatively low k_{RISC} values can be attributed to the large ΔE_{ST}. The above results indicate that these novel blue emitters can be promising candidates as emission layers in OLEDs.

In view of the excellent Φ_{PL} and narrowband emission of these novel MR emitters, OLEDs were fabricated to evaluate the electroluminescence (EL) properties with the device structure of indium tin oxide (ITO)/dipyrazino[2,3-*f*:2′,3′-*h*]quinoxaline-2,3,6,7,10,11-hexacarbonitrile (HATCN) (5 nm)/4,4′-bis[*N*-(1-naphthyl)-*N*-phenylamino]biphenyl (NPB) (30 nm)/9,9′-diphenyl-9*H*,9′*H*-3,3′-bicarbazole (BCzPh) (10 nm)/mCPBC: 4TCzBN: *x* wt% emitters (EML, 24 nm)/4,6-bis(3-(9*H*-carbazol-9-yl)phenyl)pyrimidine (CzPhPy) (15 nm)/9,10-bis(6-phenylpyridin-3-yl)anthracene (DPPyA) (30 nm)/LiF (0.5 nm)/Al (150 nm). The energy diagram and the molecular

Table 1 Photophysical and electrochemical data of TMInBN, Mes-InBN, Cz-InBN, and TCz-InBN

Emitter	λ_{abs}[a] (nm)	λ_{PL}[a] (nm)	FWHM[b] (nm)	E_S/E_T[c] (eV)	ΔE_{ST}[c] (eV)	HOMO/LUMO[d] (eV)	Φ_{PL}[e] (%)	Φ_P/Φ_d[f] (%)	τ_p/τ_d[g] (ns)/(μs)	k_r[h] (10^7 s^{-1})	k_{ISC}[h] (10^6 s^{-1})	k_{RISC}[h] (10^4 s^{-1})
TMInBN	462	475	23	2.61/2.22	0.39	−5.35/−2.54	66	49/17	5.5/14.7	8.9	93	4.6
Mes-InBN	461	475	23	2.61/2.21	0.40	−5.38/−2.52	70	42/28	6.9/24.5	6.1	84	4.6
Cz-InBN	457	470	22	2.64/2.23	0.41	−5.51/−2.58	66	43/23	5.5/15.8	7.8	104	5.9
TCz-InBN	456	470	22	2.64/2.22	0.42	−5.52/−2.56	69	45/24	5.7/17.9	7.9	96	5.4

[a] Measured in toluene (1×10^{-5} M). [b] Full width at half maximum of the fluorescence spectra in solution. [c] Obtained from the peak of the fluorescence and phosphorescence spectra in toluene. $\Delta E_{ST} = E_S - E_T$. [d] Obtained from differential pulse voltammograms (DPV) based on the peak potentials of the first oxidative and reductive waves, respectively. [e] Absolute photoluminescence quantum yield evaluated using an integrating sphere. [f] Fractional quantum yields for prompt (Φ_p) and delayed fluorescence (Φ_d). [g] Prompt (τ_p) and delayed (τ_d) emission lifetime. [h] Rate constant of fluorescence radiative decay $k_r = \Phi_p/\tau_p$, intersystem crossing $k_{ISC} = (1 - \Phi_p)/\tau_p$ and reverse intersystem crossing $k_{RISC} = \Phi_d/(k_{ISC} \cdot \tau_p \cdot \tau_d \cdot \Phi_p)$.

structures are depicted in Fig. S12 (ESI†). Among the materials used, HATCN and NPB were employed as the hole injection and transporting materials while LiF and DPPyA were used as the electron injection and transporting materials, respectively. Meanwhile, BCzPh and CzPhPy were used as the exciton-blocking compounds. In addition, mCPBC was selected as the host for the emitting layer because of its high triplet energy and wide energy band gap.[45,46] Considering the relatively low k_{RISC} of these emitters, in our devices, a TADF sensitizer was adopted to assist the triplet harvesting, which has been a routine strategy for B,N-type MR emitters.[47,48] Here, 2,3,5,6-tetrakis[3,6-bis(1,1-dimethylethyl)-9*H*-carbazol-9-yl]-benzonitrile (4TCzBN) was chosen as the TADF sensitizer owing to its relatively efficient RISC process and the proper emission to enhance the spectral overlap with the absorption of the MR emitters for efficient energy transfer (Fig. S13, ESI†). The concentration of the sensitizer was optimized to be 30 wt%, while the concentration of emitters was optimized in the range of 1–4 wt%. The current density and luminance *versus* voltage (*J*–*V*–*L*) characteristics, current efficiency (CE)/power efficiency (PE)/EQE *versus* luminance characteristics, and EL spectra are presented in Fig. 4 and Fig. S14–S17 (ESI†), and the detailed device parameters are summarized in Table 2.

As illustrated in Fig. 4a–d, the EL spectra of the OLED devices show the main emission from the MR emitters. The emission of the sensitizer completely vanishes when the dopant concentration is above 1 wt%, suggesting the efficient energy transfer. Obvious red-shifted emission peaks from sky-blue (480 nm) to bluish-green (489 nm) are observed for the TMInBN-based devices with increased dopant concentrations. Meanwhile, the FWHMs are also clearly enlarged from 31 nm to 68 nm. These behaviours are similar to the photophysical results in doped films as illustrated in Fig. S5 (ESI†). The reason is assigned to the aggregation effect of TMInBN in the solid state given its planar structure. In contrast, the doped devices based on the other three compounds display nearly identical emission peaks and FWHMs with increased dopant concentrations, suggesting that the steric substituents of these emitters can sufficiently inhibit molecular aggregation in the doped films.

The EQE–luminance characteristics are provided in Fig. 4e–h. Only an EQE_{max} of 9.0% is observed for TMInBN and the value is sharply reduced with increased dopant concentrations. We attribute this phenomenon to the strong intermolecular interactions in doped films, which can lead to aggregation-induced quenching. Notably, with the introduction of steric substituents, the EQE_{max} of the other three emitters are greatly improved, and the aggregation-induced quenching issue is well suppressed with increased dopant concentrations. The highest EQE_{max} of 16.8% is observed for the Cz-InBN-based device, together with a small FWHM of 29 nm and the Commission Internationale de d'Éclairage (CIE) coordinate of (0.13, 0.20). We believe that the device performance can be further improved by rational

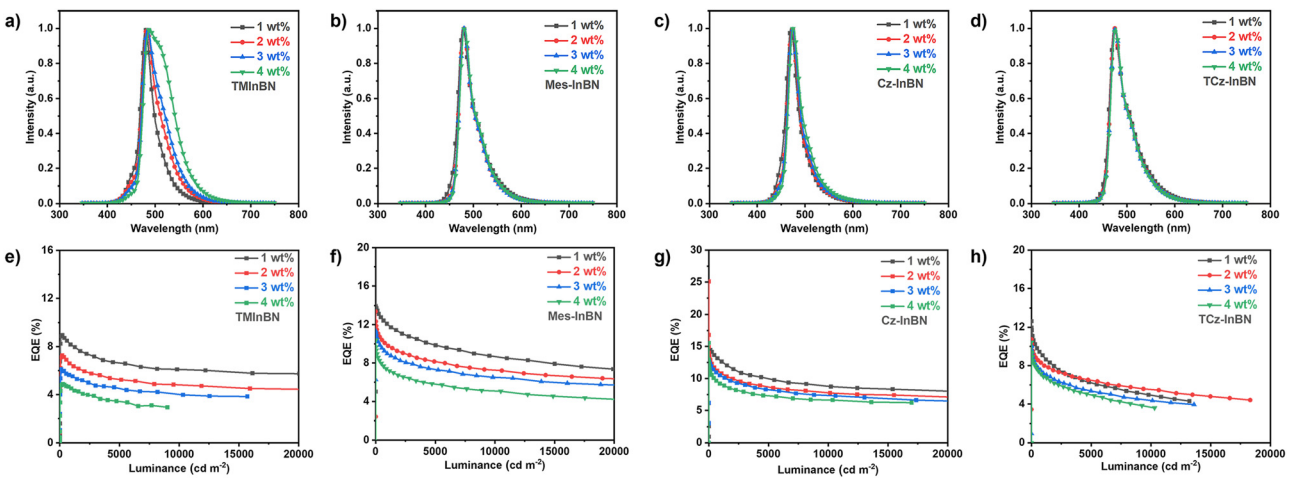

Fig. 4 (a–d) The EL spectra and (e–h) the EQE–luminance curves of the OLED devices based on TMInBN, Mes-InBN, Cz-InBN, and TCz-InBN.

Table 2 Summary of the OLED device performance of TMInBN, Mes-InBN, Cz-InBN, and TCz-InBN

Emitter	x wt (%)	λ_{EL}[a] [nm]	FWHM[b] [nm]	CE_{max}[c] [cd A^{-1}]	PE_{max}[d] [lm W^{-1}]	EQE_{max}[e] [%]	CIE(x,y)
TMInBN	1	480	31	14.7	10.9	9.0	0.13,0.26
	2	483	42	15.1	11.1	7.3	0.15,0.36
	3	485	50	14.2	10.1	6.1	0.16,0.41
	4	489	68	13.3	9.4	4.9	0.19,0.50
Mes-InBN	1	479	40	27.8	29.1	13.9	0.15,0.32
	2	481	35	24.6	27.6	13.4	0.14,0.34
	3	481	34	23.5	26.3	11.4	0.14,0.35
	4	482	35	21.3	23.9	10.4	0.14,0.37
Cz-InBN	1	470	30	18.8	14.1	14.5	0.14,0.17
	2	474	29	22.5	20.8	16.8	0.13,0.20
	3	474	29	19.8	16.4	12.7	0.13,0.22
	4	476	31	20.8	19.3	13.0	0.14,0.25
TCz-InBN	1	473	45	24.4	27.3	12.6	0.16,0.31
	2	475	42	30.2	36.5	10.8	0.15,0.31
	3	475	40	20.7	23.1	10.1	0.15,0.32
	4	477	40	18.7	19.5	10.4	0.15,0.32

[a] The EL peak. [b] Full width at half maximum. [c] Maximum current efficiency. [d] Maximum power efficiency. [e] Maximum external quantum efficiency.

structural modification or device optimization, such as introducing suitable substituents, utilizing assistant dopants, or optimizing the device configurations.[27,36,47,49–53]

In conclusion, we have designed and synthesized a novel MR-TADF emitter based on indole (InBN) *via* π-truncation of the representative carbazole-fused MR skeleton CzBN. Using InBN as the parent skeleton, a series of blue-emitting MR-TADF materials have been developed by peripheral substitution engineering, finally affording high quantum yields and excellent color purity (FWHMs: 22–23 nm). The TADF-sensitized OLEDs employing these emitters exhibited sharp blue emission with the smallest FWHM of 29 nm and the highest EQE_{max} of up to 16.8% simultaneously. This work not only provides a novel molecular design strategy to expand the molecular diversity of MR emitters, but also motivates the exploration of BN-heteroarenes with multicolor narrowband emission.

Conflicts of interest

There are no conflicts to declare.

Acknowledgements

We acknowledge the financial support from the National Natural Science Foundation of China (No. 92256304 and 22071120), the National Key R&D Program of China (2020YFA0711500), the Open Fund of the State Key Laboratory of Luminescent Materials and Devices (South China University of Technology), and the Fundamental Research Funds for the Central Universities.

Notes and references

1 E. Peli, *ITU-R Recommendation BT, 2020: Parameter Values for Ultrahigh Definition Television Systems for Production and International Programme Exchange*, *International Telecommunication Union*, *Geneva*, 2012.
2 H. Uoyama, K. Goushi, K. Shizu, H. Nomura and C. Adachi, *Nature*, 2012, **492**, 234–238.
3 F. Santoro, A. Lami, R. Improta, J. Bloino and V. Barone, *J. Chem. Phys.*, 2008, **128**, 224311.
4 Y. Kondo, K. Yoshiura, S. Kitera, H. Nishi, S. Oda, H. Gotoh, Y. Sasada, M. Yanai and T. Hatakeyama, *Nat. Photonics*, 2019, **13**, 678–682.
5 T. Hatakeyama, K. Shiren, K. Nakajima, S. Nomura, S. Nakatsuka, K. Kinoshita, J. Ni, Y. Ono and T. Ikuta, *Adv. Mater.*, 2016, **28**, 2777–2781.
6 S. Madayanad Suresh, D. Hall, D. Beljonne, Y. Olivier and E. Zysman-Colman, *Adv. Funct. Mater.*, 2020, **30**, 1908677.
7 J.-M. Teng, Y.-F. Wang and C.-F. Chen, *J. Mater. Chem. C*, 2020, **8**, 11340–11353.
8 C. Chen, C.-Z. Du and X.-Y. Wang, *Adv. Sci.*, 2022, **9**, e2200707.
9 T. Fan, Y. Zhang, D. Zhang and L. Duan, *Chem. – Eur. J.*, 2022, **28**, e202104624.
10 R. K. Konidena and K. R. Naveen, *Adv. Photonics Res.*, 2022, **3**, 2200201.
11 W. P. Hong, H. N. Lim and I. Shin, *Synthesis*, 2022, 570–588.
12 X. Wang, Y. Zhang, H. Dai, G. Li, M. Liu, G. Meng, X. Zeng, T. Huang, L. Wang, Q. Peng, D. Yang, D. Ma, D. Zhang and L. Duan, *Angew. Chem., Int. Ed.*, 2022, **61**, e202206916.
13 S. Oda, B. Kawakami, Y. Yamasaki, R. Matsumoto, M. Yoshioka, D. Fukushima, S. Nakatsuka and T. Hatakeyama, *J. Am. Chem. Soc.*, 2022, **144**, 106–112.
14 C. Y. Chan, S. Madayanad Suresh, Y. T. Lee, Y. Tsuchiya, T. Matulaitis, D. Hall, A. M. Z. Slawin, S. Warriner, D. Beljonne, Y. Olivier, C. Adachi and E. Zysman-Colman, *Chem. Commun.*, 2022, **58**, 9377–9380.
15 S. Xu, Q. Yang, Y. Zhang, H. Li, Q. Xue, G. Xie, M. Gu, J. Jin, L. Huang and R. Chen, *Chin. Chem. Lett.*, 2021, **32**, 1372–1376.
16 Y. Xu, Z. Cheng, Z. Li, B. Liang, J. Wang, J. Wei, Z. Zhang and Y. Wang, *Adv. Opt. Mater.*, 2020, **8**, 1902142.
17 X.-F. Luo, H.-X. Ni, H.-L. Ma, Z.-Z. Qu, J. Wang, Y.-X. Zheng and J.-L. Zuo, *Adv. Opt. Mater.*, 2022, **10**, 2102513.
18 X.-F. Luo, S.-Q. Song, H.-X. Ni, H. Ma, D. Yang, D. Ma, Y.-X. Zheng and J.-L. Zuo, *Angew. Chem., Int. Ed.*, 2022, **61**, e202209984.
19 M. Yang, S. Shikita, H. Min, I. S. Park, H. Shibata, N. Amanokura and T. Yasuda, *Angew. Chem., Int. Ed.*, 2021, **60**, 23142–23147.
20 Y. Zhang, D. Zhang, J. Wei, Z. Liu, Y. Lu and L. Duan, *Angew. Chem., Int. Ed.*, 2019, **58**, 16912–16917.
21 Y.-T. Lee, C.-Y. Chan, M. Tanaka, M. Mamada, U. Balijapalli, Y. Tsuchiya, H. Nakanotani, T. Hatakeyama and C. Adachi, *Adv. Electron. Mater.*, 2021, **7**, 2001090.
22 M. Yang, I. S. Park and T. Yasuda, *J. Am. Chem. Soc.*, 2020, **142**, 19468–19472.
23 S. Oda, W. Kumano, T. Hama, R. Kawasumi, K. Yoshiura and T. Hatakeyama, *Angew. Chem., Int. Ed.*, 2021, **60**, 2882–2886.
24 Y. Xu, C. Li, Z. Li, Q. Wang, X. Cai, J. Wei and Y. Wang, *Angew. Chem., Int. Ed.*, 2020, **59**, 17442–17446.
25 Y. Liu, X. Xiao, Y. Ran, Z. Bin and J. You, *Chem. Sci.*, 2021, **12**, 9408–9412.
26 Y. Qi, W. Ning, Y. Zou, X. Cao, S. Gong and C. Yang, *Adv. Funct. Mater.*, 2021, **31**, 2102017.

27 Y. Xu, C. Li, Z. Li, J. Wang, J. Xue, Q. Wang, X. Cai and Y. Wang, *CCS Chem.*, 2021, **3**, 2077–2091.
28 F. Huang, X.-C. Fan, Y.-C. Cheng, H. Wu, Y.-Z. Shi, J. Yu, K. Wang, C.-S. Lee and X.-H. Zhang, *Mater. Horiz.*, 2022, **9**, 2226–2232.
29 P. Jiang, J. Miao, X. Cao, H. Xia, K. Pan, T. Hua, X. Lv, Z. Huang, Y. Zou and C. Yang, *Adv. Mater.*, 2022, **34**, e2106954.
30 F. Liu, Z. Cheng, L. Wan, Z. Feng, H. Liu, H. Jin, L. Gao, P. Lu and W. Yang, *Small*, 2022, **18**, e2106462.
31 Y. K. Qu, D. Y. Zhou, F. C. Kong, Q. Zheng, X. Tang, Y. H. Zhu, C. C. Huang, Z. Q. Feng, J. Fan, C. Adachi, L. S. Liao and Z. Q. Jiang, *Angew. Chem., Int. Ed.*, 2022, **61**, e202201886.
32 Y. Zhang, J. Wei, D. Zhang, C. Yin, G. Li, Z. Liu, X. Jia, J. Qiao and L. Duan, *Angew. Chem., Int. Ed.*, 2022, **61**, e202113206.
33 Y. Xu, Q. Wang, X. Cai, C. Li and Y. Wang, *Adv. Mater.*, 2021, **33**, e2100652.
34 Y. Qiu, H. Xia, J. Miao, Z. Huang, N. Li, X. Cao, J. Han, C. Zhou, C. Zhong and C. Yang, *ACS Appl. Mater. Interfaces*, 2021, **13**, 59035–59042.
35 J. Park, J. Lim, J. H. Lee, B. Jang, J. H. Han, S. S. Yoon and J. Y. Lee, *ACS Appl. Mater. Interfaces*, 2021, **13**, 45798–45805.
36 J. Han, Z. Huang, X. Lv, J. Miao, Y. Qiu, X. Cao and C. Yang, *Adv. Opt. Mater.*, 2021, **10**, 2102092.
37 X.-F. Luo, H.-X. Ni, A.-Q. Lv, X.-K. Yao, H.-L. Ma and Y.-X. Zheng, *Adv. Opt. Mater.*, 2022, **10**, 2200504.
38 R. J. Sundberg, *Heterocyclic Scaffolds II: Top. Heterocycl. Chem.*, 2010, vol. 26, pp. 47–115.
39 D. Hall, J. C. Sancho-Garcia, A. Pershin, G. Ricci, D. Beljonne, E. Zysman-Colman and Y. Olivier, *J. Chem. Theory Comput.*, 2022, **18**, 4903–4918.
40 M. Nagata, H. Min, E. Watanabe, H. Fukumoto, Y. Mizuhata, N. Tokitoh, T. Agou and T. Yasuda, *Angew. Chem., Int. Ed.*, 2021, **60**, 20280–20285.
41 H. L. Lee, S. O. Jeon, I. Kim, S. C. Kim, J. Lim, J. Kim, S. Park, J. Chwae, W. J. Son, H. Choi and J. Y. Lee, *Adv. Mater.*, 2022, **34**, 2202464.
42 K. Shizu and H. Kaji, *Commun. Chem.*, 2022, **5**, 53.
43 K. R. Naveen, H. Lee, L. H. Seung, Y. H. Jung, C. P. Keshavananda Prabhu, S. Muruganantham and J. H. Kwon, *Chem. Eng. J.*, 2023, **451**, 138498.
44 K. Stavrou, A. Danos, T. Hama, T. Hatakeyama and A. Monkman, *ACS Appl. Mater. Interfaces*, 2021, **13**, 8643–8655.
45 G. Meng, H. Dai, T. Huang, J. Wei, J. Zhou, X. Li, X. Wang, X. Hong, C. Yin, X. Zeng, Y. Zhang, D. Yang, D. Ma, G. Li, D. Zhang and L. Duan, *Angew. Chem., Int. Ed.*, 2022, **61**, e202207293.
46 P. Wei, D. Zhang and L. Duan, *Adv. Funct. Mater.*, 2020, **30**, 1907083.
47 T. Huang, Q. Wang, S. Xiao, D. Zhang, Y. Zhang, C. Yin, D. Yang, D. Ma, Z. Wang and L. Duan, *Angew. Chem., Int. Ed.*, 2021, **60**, 23771–23776.
48 C. Yin, D. Zhang, Y. Zhang, Y. Lu, R. Wang, G. Li and L. Duan, *CCS Chem.*, 2020, **2**, 1268–1277.
49 Y. Zhang, D. Zhang, T. Huang, A. J. Gillett, Y. Liu, D. Hu, L. Cui, Z. Bin, G. Li, J. Wei and L. Duan, *Angew. Chem., Int. Ed.*, 2021, **60**, 20498–20503.
50 D. Zhang, X. Song, A. J. Gillett, B. H. Drummond, S. T. E. Jones, G. Li, H. He, M. Cai, D. Credgington and L. Duan, *Adv. Mater.*, 2020, **32**, 1908355.
51 S. H. Han, J. H. Jeong, J. W. Yoo and J. Y. Lee, *J. Mater. Chem. C*, 2019, **7**, 3082–3089.
52 D. Zhang, X. Song, M. Cai and L. Duan, *Adv. Mater.*, 2018, **30**, 1705250.
53 S. O. Jeon, K. H. Lee, J. S. Kim, S.-G. Ihn, Y. S. Chung, J. W. Kim, H. Lee, S. Kim, H. Choi and J. Y. Lee, *Nat. Photonics*, 2021, **15**, 208–215.

